Chinese Chemical Letters 35 (2024) 109274

Contents lists available at ScienceDirect

Chinese Chemical Letters

journal homepage: www.elsevier.com/locate/cclet

Converting $LiNO_3$ additive to single nitrogenous component $Li_2N_2O_2$ SEI layer on Li metal anode in carbonate-based electrolyte

Kunyao Peng[a], Xianbin Wang[a], Xingbin Yan[a,b,*]

[a] Department of Materials Science and Engineering, Sun Yat-sen University, Guangzhou 510275, China
[b] State Key Laboratory of Optoelectronic Materials and Technologies, Guangzhou 510275, China

ARTICLE INFO

Article history:
Received 28 September 2023
Revised 24 October 2023
Accepted 1 November 2023
Available online 8 November 2023

Keywords:
Li metal anode
Electrolyte additive
Lithium nitrate
Solid electrolyte interphase
Carbonate electrolyte

ABSTRACT

With the increasing demand for high energy density energy storage device, Li metal has received intensive attention for its ultrahigh capacity and the lowest redox potential. $LiNO_3$ is widely used as electrolyte additive for ether electrolyte, which can improve the cycle performance of Li metal anode. Compared to ethers, carbonates are more suitable for Li metal batteries with high voltage cathode because they have a wider electrochemical window. However, $LiNO_3$ performs poor solubility in carbonate electrolyte, restricting its application in high voltage Li battery. Herein, we presented a facile method to introduce abundant $LiNO_3$ additive to carbonate electrolyte system by introducing $LiNO_3$-PAN es as the interlayer of the cell. $LiNO_3$-PAN es is in sufficient contact with the electrolyte so that it can continuously releases $LiNO_3$ to assist the formation of $Li_2N_2O_2$-rich single nitrogenous component SEI layer on Li surface. With the help of $LiNO_3$-PAN es, Li metal anode shows excellent cycle stability even at a high current density of 4 mA/cm^2, so that the cycle performance of the full cells was significantly improved, whether in the anode-free Cu||LFP cell or the Li||NCM622 cell.

Rechargeable lithium ion batteries have been world-widely used as energy storage devices in electronic vehicles and digital products [1]. However, the Li-ion batteries are difficult to meet the increasing demand for high energy density energy storage system because the capacity of the traditional anode materials is gradually approaching to its theoretical value [2]. In recent years, metallic lithium has been revived and is considered as the next generation anode material due to its high specific capacity (3860 mAh/g) and the lowest electrochemical reduction potential (−3.04 V *vs.* standard hydrogen electrode).

Despite the superior properties of Li metal, the uncontrollable Li dendrite growth during the Li strip/deposit process makes Li metal anode perform a low coulombic efficiency, leading to the poor cycle performance of the Li metal battery, which restricts the commercialization of the Li metal anode. And the Li dendrite problem is particularly severe in carbonate-based electrolyte. Various strategies have been developed to suppress Li dendrite growth and improve the cycle stability of Li metal anode. The mainstream strategies for Li anode protection are using lithiophilic conductive host as current collector [3–5], regulating electrolyte solvent [6–8], and constructing stable solid electrolyte interface (SEI) layer on Li surface [9,10], *etc.* Among these strategies, modifying SEI layer is one of the most resultful strategies for it is a direct way to homogenize the Li-ion flux on the Li anode surface, which can alleviate the uneven Li deposition and suppress the growth of Li dendrites [10–12].

Various strategies have been developed to construct stable SEI layer on Li metal anode's surface. The SEI layers are usually modified by ex-situ reactions with Li metal [13–16], or optimizing the SEI component with electrolyte additives such as fluoroethylene carbonate (FEC), vinylene carbonate (VC) and $LiNO_3$ [17–20]. Among these electrolyte additives, $LiNO_3$ has been considered as an effective additive in ether-based electrolytes, due to its formation of stable SEI layer on Li metal anode surface. The SEI layer is enriched with various of nitrogenous compound LiN_xO_y (where LiN_xO_y refers to any $LiNO_3$ reduction products, including Li_3N, $LiNO_2$, and $Li_2N_2O_2$) [20,21]. However, Li metal batteries should use the cathode with higher redox potential for achieving a higher energy density of the full cell, while traditional ether-based electrolyte is difficult to meet the demand due to its narrow electrochemical window [22,23] Carbonate electrolytes are electrochemically stable at high voltage, but $LiNO_3$ behaves poor solubility in carbonates even after the addition of other cosolvents or coordination dissolution promotors [24,25]. Therefore, exploring the way to

* Corresponding author.
E-mail address: yanxb3@mail.sysu.edu.cn (X. Yan).

https://doi.org/10.1016/j.cclet.2023.109274
1001-8417/

introduce abundant $LiNO_3$ into carbonate electrolyte is an important direction for SEI modification strategy of Li metal anode.

A variety of theoretical models for SEI layer have been proposed, including multilayer model and mosaic model, and the mosaic model is by far well accepted and confirmed by various experiments [26–29]. The mosaic structure of SEI layer would lead to inhomogeneous Li^+ flux, which cause internal local stress, SEI rupture on Li anode surface, and eventually leads to Li dendrite growth. Instead, a homogenous SEI layer can homogenize the Li^+ flux, thereby achieving an improvement of the cycle performance of Li anode. Therefore, the structural uniformity of SEI is more decisive than its mechanical strength [30]. So far, $LiNO_3$ are found possible to be abundantly introduced into carbonate electrolyte *via* a slow-release method, which is simply dispersed $LiNO_3$ on porous separator [31,32], or absorbed in MOF nanoparticle host and separated it into electrolyte [33]. Although these reported strategies is effective to improve the cycle stability of Li anode, the SEI component constructed by $LiNO_3$ are multifold, which is opposite to the requirement that homogenize the SEI component. And a method that converts $LiNO_3$ additive into a single SEI component is barely reported.

Herein, we apply a strategy that allows $LiNO_3$ to be continuously introduced into carbonate electrolyte *via* a slow-release design realized by $LiNO_3$-PAN electrospinning ($LiNO_3$-PAN es) nanowire interlayer (Fig. 1). Using electrospinning technique, $LiNO_3$ additive is abundantly dissolved in PAN electrospinning nanowire cloth, which is beneficial for contacting with carbonate electrolyte and continuously releasing $LiNO_3$ into electrolyte to form a single $Li_2N_2O_2$ nitrogenous SEI on Li surface. Compared with other $LiNO_3$ addition strategies, this strategy can introduce more $LiNO_3$ than the dissolution promotors strategy and does not require the use of $LiNO_3$ host with high mass (such as GF separator), which is more advantageous in terms of the amount of $LiNO_3$ addition and the energy density of the battery. With the help of $LiNO_3$-PAN electrospinning nanowire interlayer, the dendrite formation of Li metal anode was inhibited by $Li_2N_2O_2$-rich SEI protective layer, the surface of Li anode can remain stable even when operated at high current density of 4 mA/cm^2. This strategy not only provides a facile way to introduce a large amount of $LiNO_3$ into the carbonate electrolyte of Li metal batteries, but also discovers that most of the $LiNO_3$ can be converted to a single nitrogen-containing SEI component $Li_2N_2O_2$ when coordinated with PAN. This work demonstrates the possibility of constructing a single nitrogenous SEI component $Li_2N_2O_2$ from $LiNO_3$ in carbonate electrolyte, which is beneficial for improving the homogeneity of the SEI layer and the cycle performance of Li metal batteries.

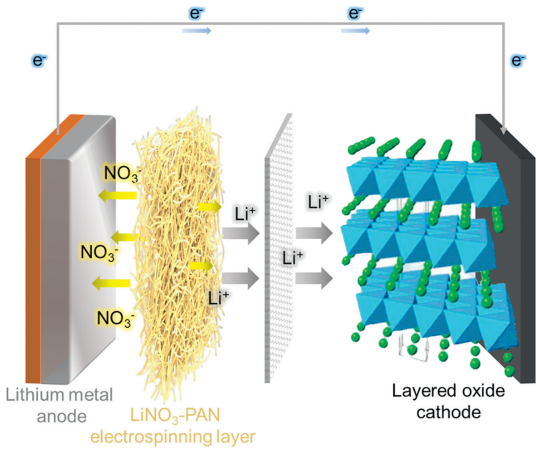

Fig. 1. The schematic diagram of $LiNO_3$-PAN es layer used as the interlayer of Li metal battery, which can continuously release $LiNO_3$ to electrolyte to protect Li metal anode.

The $LiNO_3$-PAN es nanowire cloth was synthesized by electrospinning technique. 0.5 g of $LiNO_3$ solid particles was dissolved in 10 mL of *N*,*N*-dimethylformamide (DMF), and subsequently, 0.5 g of PAN was added to the solution under vigorous stirring conditions to form the electrospinning solution. The electrospinning device we used is Ucalery ET-2535H (Fig. S1 in Supporting information), which is airtight and able to control the operating temperature and humidity. The electrospinning process needs to control the environment condition to a temperature of 40–45 °C, and a relative humidity below 50%. The electrospinning process was shown in Fig. S1. 8 mL of $LiNO_3$-PAN electrospinning solution was extracted in a 10 mL syringe, and assembled on the booster of the electrospinning device. A4 printing paper was attached to the surface of the metal roller electrospinning collector. An electrostatic positive voltage of about +18 kV was applied at the needle of the solution, and a negative voltage of about −1.5 kV was applied at the collector to fabricate the electrospinning nanowire. The distance between the collector and the syringe ranged from 18 cm to 25 cm, and the rotational speed of the roller collector was 140 r/min. The synthesized $LiNO_3$-PAN es required vacuum drying at 120 °C for 12 h to remove the H_2O absorbed on the material during the electrospinning process, preventing the moisture from harming Li battery's electrochemical performance. The weight of $LiNO_3$-PAN es interlayer is ~2.5 mg/cm^2, containing 50 mass% of the $LiNO_3$ additive, which is equivalent to adding ~12 mol/L of $LiNO_3$ if the amount of electrolyte is 100 μL/cm^2.

Phase structure was characterized *via* XRD analysis by Rigaku DMAX 2200 VPC X-ray diffractometer (Japan) using Cu Kα radiation ($\lambda = 1.54056$ Å). Infrared spectra were tested using the attenuated total reflection (ATR) mode of the Thermo Fisher Nicolet iS50 FTIR microscopy. The microcosmic morphology of Li metal anode surface and $LiNO_3$-PAN es were characterized by SEM (COXEM, EM-30AX plus, Korea).

Electrochemical measurements were carried out using two electrodes CR2032-type coin cells. Li metal foil was purchased from China Energy Lithium Co., Ltd. and reserved in Ar glove box (H_2O, $O_2 < 0.1$ ppm). Li metal foil required the removal of the surface oxide layer by scalpel and roll-pressed to a fresh Li foil with a unified thickness of 0.35–0.40 mm, and finally cut into 11.5 mm diameter (1 cm^2 area) discs preserved as Li metal anode. The electrolyte this manuscript used was 1 mol/L $LiPF_6$ in EC/DMC/EMC (vol%: 1:1:1), and the amount of the electrolyte used in battery is 100 μm. The cycle performance of cell was tested by LANHE CT2001A battery test device. The loading mass of $LiFePO_4$ cathode in the full cell test is ~2.9 mg/cm^2, the loading mass of NCM622 cathode in the full cell test is ~23 mg/cm^2, and the area of cathode is 1.13 cm^2. The EIS tests were carried out by Autolab electrochemical work station. The frequency range of EIS test is 100,000 Hz to 1 Hz, and the amplitude is ±10 mV.

As shown in Fig. 2a, the $LiNO_3$-PAN es interlayer (Fig. 2b) is synthesized by electrospinning technique. To remove the small amount of moisture absorbed by $LiNO_3$ during the electrospinning process, the obtained $LiNO_3$-PAN es is dried at 80 °C under vacuum for 24 h before being used as battery interlayer. As shown by the SEM image of $LiNO_3$-PAN es in Figs. 2c and d, $LiNO_3$ is uniformly dispersed in PAN electrospinning nanowires with a diameter of 500–700 nm, no crystal or bulk structure is observed. And the XRD pattern of $LiNO_3$-PAN es (Fig. S2 in Supporting information) is consistent with pure PAN's one, no diffraction peak of $LiNO_3$ crystal was observed, which means that the $LiNO_3$ of $LiNO_3$-PAN es electrospinning nanowires was dissolved in PAN polymer instead of mixing with PAN polymer.

For characterizing the chemical environment of $LiNO_3$ in the $LiNO_3$-PAN es interlayer, we perform the infrared spectroscopy (IR)

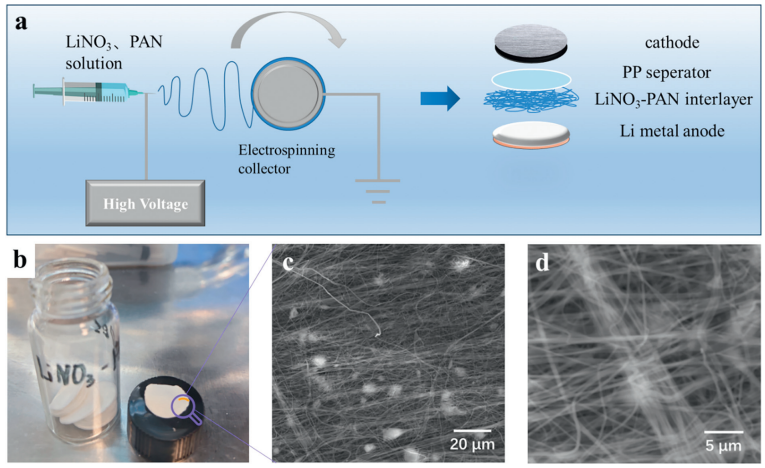

Fig. 2. (a) Schematic configurations of the synthesis process of the $LiNO_3$-PAN es. (b) The synthesized $LiNO_3$-PAN es interlayer was 16 mm in diameter. (c, d) The SEM image of $LiNO_3$-PAN es interlayer cloth.

and XPS tests on the prepared $LiNO_3$-PAN es and PAN comparing group. Due to the nanostructure of $LiNO_3$-PAN es, it is macroscopically opaque and its IR cannot be measured in transmission mode. Therefore, we use the attenuated total reflection (ATR) mode to test the electrospinning cloth samples. In the ATR-FTIR spectroscopy of $LiNO_3$-PAN es (Fig. S3a in Supporting information), we can observe an asymmetric stretching vibration peak of C–H bond of methylene group at 2923 cm^{-1}, a stretching vibration peak of cyan group at 2246 cm^{-1}, and a stretching vibration peak of C=C bond at 1461 cm^{-1}. The C=C bonds observed in these two samples originate from the conjugated structure formed by the dehydrogenation and cyclisation reaction of the PAN polymer during the heating process (the reaction process is shown in Fig. S3b in Supporting information). From the XPS test result, it can be noticed that the peak at 284.5 eV in the C 1s XPS spectra (Fig. S4 in Supporting information) represents sp^2 C in the sample, and the result also indicates that $LiNO_3$-PAN es contains more C=C bond structure compared to normal PAN cloth. The broad peak at 2246 cm^{-1} represents the crystalline H_2O, which is from the absorbed water during the IR test. Most of the PAN relative peaks in IR spectrum of $LiNO_3$-PAN es are consistent with the spectrum of pure PAN. The broad peak of $LiNO_3$-PAN es at 1359.6 cm^{-1} represents NO_3^-, and the NO_3^- peak also observed in N 1s XPS spectra (Fig. S4), indicating the presence of $LiNO_3$ in $LiNO_3$-PAN es. The peak of C=C bond in these two samples come from the conjugated structure formed by the dehydrogenation and cyclization reaction of PAN (Fig. S3b) during the heating process [34,35]. It is noteworthy that the peak of the C=C bond in $LiNO_3$-PAN es is red shifted compared with pure PAN, supposed to be due to the coordination between the Li^+ of $LiNO_3$ and the lone pair electrons of the N in the oxidized and cyclized PAN polymer. The XPS spectra of $LiNO_3$-PAN es (Fig. S4) also confirm the interaction between $LiNO_3$ and PAN. From the Li 1s spectra, we can learn that the peak of $LiNO_3$ in $LiNO_3$-PAN es is 55.4 eV, which is lower than the standard peak of $LiNO_3$ solid (55.8 eV). The lower binding energy of Li in $LiNO_3$-PAN es should be attributed to the dissolution of $LiNO_3$ in the PAN and the coordination between Li^+ and N of PAN.

To evaluate the effectiveness of $LiNO_3$-PAN es as an interlayer on the cycle performance of the Li metal anode in carbonate electrolyte, we assembled the Li symmetric cells and performed the cycle test at different current densities. As shown in Fig. 3a, when operated at a current density of 1 mA/cm^2 and a fixed capacity of 1 mAh/cm^2, Li symmetric cell's overpotential increased during the cycles, growing from 57.3 mV at 20 h, to a severe overpotential of 306.2 mV at 300 h. Instead, the Li symmetric cell with $LiNO_3$-PAN es performs a lower overpotential (~36.5 mV) as well as significantly improved cycle performance, which can stably cycle for over 500 h. The SEM images of Li anode after cycling (Figs. 3c and d) also show that, with the help of $LiNO_3$-PAN es, the surface morphology of Li metal anode was well maintained, no dendrites or cracks were observed after several cycles. What's more, even at a high current density of 4 mA/cm^2, the Li anode with $LiNO_3$-PAN es protection can show improved cycling stability, being able to cycle stably for 120 h (Fig. 3b), a cycle life that is much higher than the comparison group (~60 h). It also remains a dendrite-free surface comparing with the blank group (Fig. 3e) after several cycles at a high current density of 4 mA/cm^2 (Fig. 3f), which proves that $LiNO_3$-PAN es can effectively improve both the interface stability and the cycle performance of the Li metal anode.

Through the cycle tests and morphological observation of Li symmetric cell at different current densities, we found that the introduction of $LiNO_3$-PAN es can stabilize Li metal anode's surface and improve its cycle performance. To further investigate the effect of $LiNO_3$-PAN es on the surface properties of Li metal anode, we characterized the X-ray photoelectron spectroscopy (XPS) of Li symmetric cell after cycles. In the Li 1s and N 1s XPS spectra (Figs. 4a and b), signals corresponding to $Li_2N_2O_2$ can be observed when introducing $LiNO_3$-PAN es interlayer. Fig. 4a shows that the Li 1s peak of the SEI component on normal Li anode is mainly the signal of $ROCO_2Li$ (54.9 eV), which represents the deposition product of carbonate solvent. And with the help of $LiNO_3$-PAN es, the $ROCO_2Li$ peak decreased, and the newly formed Li-N peak (55.5 eV) is comparable to the $ROCO_2Li$ peak. From the N 1s and O 1s XPS spectra (Figs. 4b and c), we can also find that, after introducing $LiNO_3$-PAN es, the content of $Li_2N_2O_2$ (399.5 eV) on Li anode's SEI layer is significantly increased, which is contributed to the continuous supply of $LiNO_3$ from the $LiNO_3$-PAN es interlayer. The minor chemical signature of $Li_2N_2O_2$ and Li_3N on Li surface (Fig. 4b) comes from the N_2 in the atmosphere exposed during the XPS sample transference, which would not affect its comparison with experiment group and the conclusion. In summary, $LiNO_3$ in the $LiNO_3$-PAN es interlayer can release into carbonate electrolyte and form a single nitrogenous $Li_2N_2O_2$ on Li anode surface as SEI component to stabilize Li anode's surface. This is distinct from the currently reported results of $LiNO_3$ as an electrolyte additive, which produce multiple reduction products such as Li_3N, $LiNO_2$, and $Li_2N_2O_2$ [31,36]. The single nitrogenous $Li_2N_2O_2$ SEI formed by $LiNO_3$-PAN es interlayer possesses better uniformity compared with the works that form multiple nitrogenous components, which can facilitate the uniform depositing/stripping of Li^+ on Li metal anode's surface,

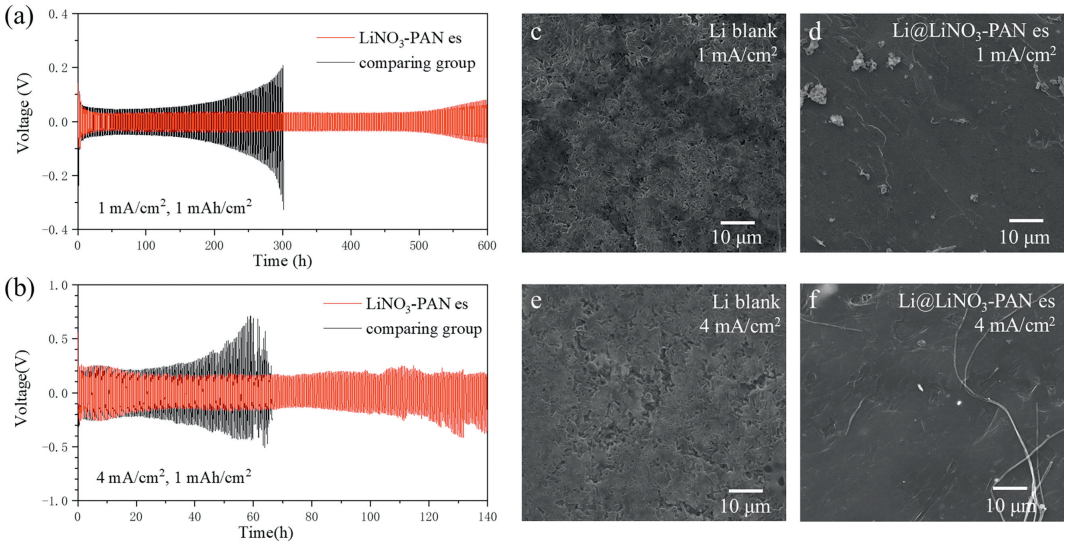

Fig. 3. The electrochemical performance of Li||Li symmetrical cell cycle test at (a) current density of 1 mA/cm^2 with Li capacity of 1 mAh/cm^2 and (b) current density of 4 mA/cm^2 with Li capacity of 1 mAh/cm^2. SEM image of pristine Li foil after 50 cycles and Li foil covered with $LiNO_3$-PAN es interlayer after 50 cycles at a current density of (c, d) 1 mA/cm^2 and (e, f) 4 mA/cm^2.

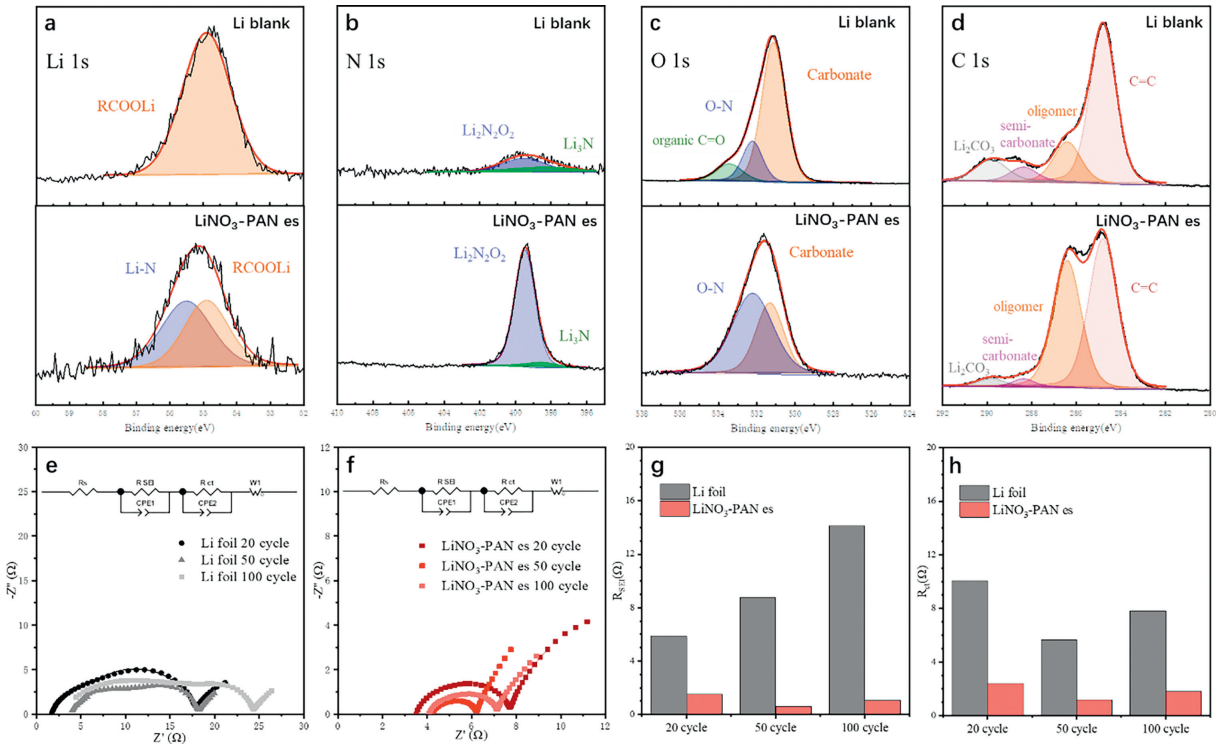

Fig. 4. XPS spectra of (a) Li 1s, (b) N 1s, (c) O 1s, (d) C 1s of Li metal anode with $LiNO_3$-PAN es covered after 50 cycles at a current density of 1 mA/cm^2 and a fixed capacity of 1 mAh/cm^2 in carbonate electrolyte. EIS Nyquist diagram of Li symmetric cells of (e) bare Li metal anode and (f) $LiNO_3$-PAN es covered Li metal anode in different cycles. The plots and the curves are the experimental and the corresponding fitting results, respectively. (g, h) The R_{SEI} and R_{ct} fitting result of Li symmetric cell of bare Li metal anode and $LiNO_3$-PAN es covered Li metal anode.

so as to stabilize the SEI layer and promote the cycle performance of the Li anode even working at high current density [30].

Besides, the SEI layer constructed by $LiNO_3$-PAN es can also alleviate the side reactions between Li metal anode and electrolyte. From the C 1s XPS spectra (Fig. 4d), we can learn that the SEI layer of Li metal anode protected by $LiNO_3$-PAN es contains less carbonate decomposition products (Li_2CO_3 and semi-carbonate) compared to the bare Li anode. The peaks of oligomers in the experimental group Li anode are higher compared to the control group, which may be due to the residual PAN polymer of $LiNO_3$-PAN es on the Li metal surface. The reduction of carbonate electrolyte-relative SEI component proves that, the SEI layer reinforced by $LiNO_3$-PAN es can effectively stabilize Li anode's surface, alleviate the side reaction between the Li metal anode and the electrolyte, thereby reducing the consumption of the electrolyte during the battery cycle and improving the cycle performance of Li metal battery.

To further analyze the interfacial stability of Li metal anode during cycling, we assembled the Li symmetric cell with $LiNO_3$-PAN es protection, and performed the electrochemical impedance spectroscopy (EIS) test after charging/discharging at a current den-

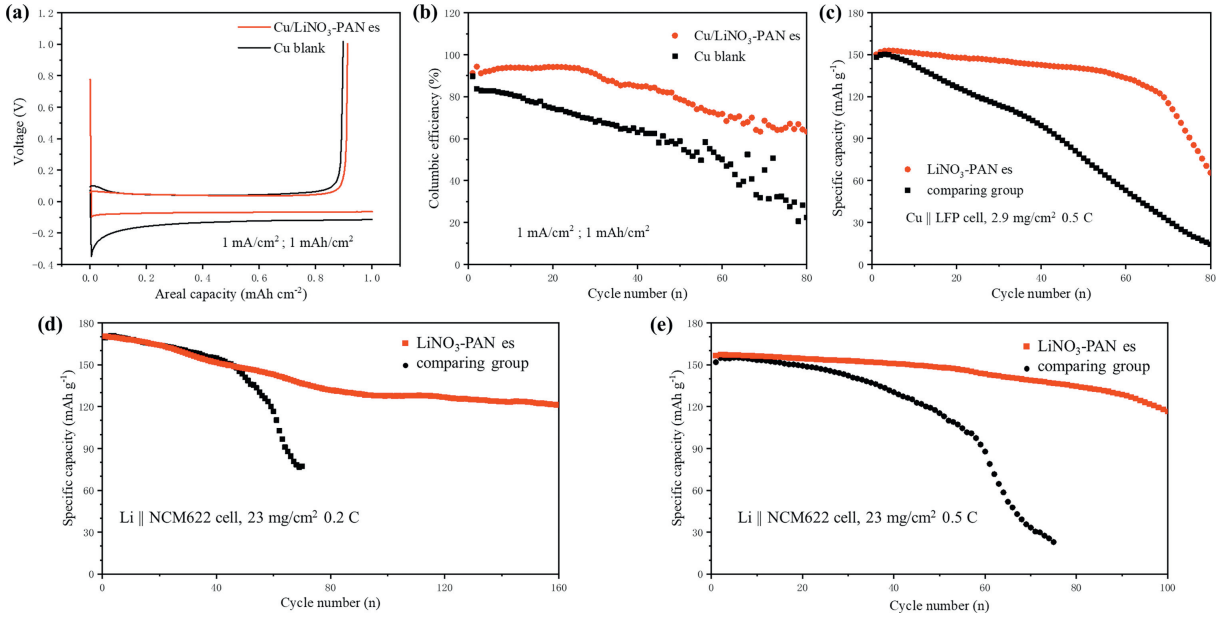

Fig. 5. (a) The Li^+ electrodepositing/stripping curve of Li||Cu cell and Li||$LiNO_3$-PAN es|Cu cell, and (b) their corresponding coulombic efficiency. (c) The Cu||LPF full cell that used Cu foil covered with $LiNO_3$-PAN es interlayer as current collector for Li deposition. (d, e) The cycle performance of NCM622||Li full cell with $LiNO_3$-PAN es interlayer added.

sity of 1 mA/cm^2 with a fixed capacity of 1 mAh/cm^2 for 20, 50, and 100 cycles, respectively. The EIS test results are shown in Figs. 4e and f. In the Nyquist diagram of Li symmetric cell, the high-frequency region corresponds to the Li^+ migration impedance of the electrodes (R_{SEI}), which is determined by the SEI layer on the surface of Li anode, and the mid- and low-frequency regions correspond to the charge transfer impedance of the electrodes (R_{ct}), which corresponds to the charge transfer process of the Li anode. Subsequently, we fitted the EIS results with the artificial circuit model in Figs. 4e and f, to obtain R_{SEI} and R_{ct} of Li anode. The R_{SEI} of Li symmetric cell during different cycles are shown in Fig. 4g. When the Li symmetric cell anode operated, the Li anode's interface impedance R_{SEI} increases from 5.89 Ω at 20 cycles to 8.75 Ω at 50 cycles and 14.11 Ω at 100 cycles, which is due to the continuous growth of Li dendrites and the repetitive fracture and generation of SEI during charge/discharge process. After introducing $LiNO_3$-PAN es on Li surface, the R_{SEI} of Li metal anode did not change significantly during the long cycle test, from 1.52 Ω at 20 cycles to 0.62 Ω at 50 cycles and 1.05 Ω at 100 cycles. This indicates that with the assistance of $LiNO_3$-PAN es, a $Li_2N_2O_2$-rich SEI protective layer was constructed on Li anode's surface, so that the stability of the SEI layer was significantly improved, and the R_{SEI} of Li metal anode can remain stable during the cycle tests. Li anode with $LiNO_3$-PAN es protection also performs a lower R_{ct} (Fig. 4h) during the long cycle tests, which also reveals that when the Li anode is constructed with the $Li_2N_2O_2$-rich SEI protective layer, the kinetics of the Li^+ deposition reaction of Li metal anode was improved.

From the previous analysis and characterization, we know that $LiNO_3$-PAN es can promote the cycle performance of Li metal anode by constructing a $Li_2N_2O_2$-rich SEI layer to homogenize the deposition of Li^+ on Li anode's surface. To evaluate the effect of $LiNO_3$-PAN es on Li deposition behavior, we use Cu foil as the current collector for Li deposition, and test its electrochemical performance. The Li electrodepositing and stripping curve of Li||Cu cell with $LiNO_3$-PAN es introduced was shown in Fig. 5a. The Li nucleation electrochemical potential of Cu/$LiNO_3$-PAN es at the first cycle is 98.5 mV, and the Li deposition potential is 68.8 mV, which is much lower than the bare Cu current collector's Li nucleation potential (348.1 mV) and deposition potential (127.1 mV), indicating that the nanostructure of $LiNO_3$-PAN es can homogenize the Li^+ flux and decrease the energy barrier of Li nucleation and deposition. The Li||Cu cycle test (Fig. 5b) shows that, although the coulombic efficiency (CE) of the Cu/$LiNO_3$-PAN current collector has not reached a practical value (> 99%), it also has a clear improvement compared with ordinary Cu foil in the early stage of the cycles. It is presumed that the inferior cycle performance enhancement of $LiNO_3$-PAN es in the Li||Cu cell compared to the Li symmetric cell is because $LiNO_3$-PAN es need to contact with Li metal to form a $Li_2N_2O_2$-rich SEI protective layer. However, there is no Li metal on Cu foil's surface to react initially, and the newly deposited Li tends to form Li dendrites, so that the released $LiNO_3$ is difficult to construct a stable SEI protective layer on the Cu current collector.

To evaluate the effect of $LiNO_3$-PAN es on the performance of lithium metal battery, we used Li metal anode and Cu foil current collector as anode, to assemble Li metal battery and perform the cycle tests. Due to the unsatisfactory performance of the previously tested Cu||Li cell, we use the $LiFePO_4$ cathode with a low loading mass (2.9 mg/cm^2) for the cycle performance test. The cycle performance of the anode-free Cu||$LiFePO_4$ full cell using a Cu foil current collector modified with $LiNO_3$-PAN es is shown in Fig. 5c, which was tested at a C-rate of 0.5 C, corresponding to a current density of 0.232 mA/cm^2. Since this is an anode-free system, the Li metal of the anode comes from the Li^+ that released during the charging (delithiation) process of the $LiFePO_4$, and the cycle performance of the $LiFePO_4$ cathode is much better than Cu foil anode for Li deposition reaction. Therefore, the cycle performance of the Cu||$LiFePO_4$ system is mainly depends on the CE of the Li deposit/strip reaction of the Cu foil anode. The cycle performance result (Fig. 5c) shows that, after introducing $LiNO_3$-PAN es interlayer, the average CE of the full cell in the initial 50 cycles is 99.38%, much higher than the comparing group (97.15%). The well-improved cycle stability of Cu||$LiFePO_4$ cell caused by $LiNO_3$-PAN es can maintain for about 60 cycles, while the cycle performance of the control group was less satisfactory from the beginning of the operation, resulting in a rapid decay of the battery capacity. In conclusion, with the help of $LiNO_3$-PAN es, the Li strip/deposit CE of the Cu foil current collector was significantly improved, so

that the cycle performance of Cu||$LiFePO_4$ full cell was effectively enhanced as well.

Subsequently, we test the cycle performance of Li||NCM622 cell to evaluate the positive effect of $LiNO_3$-PAN es on the Li metal battery full cell. Since the $LiNO_3$-PAN es can significantly improve the cycle stability of Li metal anode even operated at high current density, we used a high loading mass (23 mg/cm^2) NCM622 electrode as cathode of the full cell and cycled at C-rate of 0.2 C and 0.5 C, which corresponds to a current density of 0.8 mA/cm^2 and 2 mA/cm^2, respectively. The results are shown in Figs. 5d and e. When Li||NCM622 with $LiNO_3$-PAN es introduced was operated at a rate of 0.2 C, its specific capacity decreased from 170 mAh/g to 121 mAh/g with a capacity retention of 71.2% after 160 cycles; when operated at a rate of 0.5 C, its specific capacity decreased from 155 mAh/g to 118 mAh/g with a capacity retention of 76.1% after 100 cycles, both of which are better than the comparing group. These results prove that the cycle performance of Li || NCM622 full cells is significantly improved after the introduction of $LiNO_3$-PAN es interlayer due to the stable SEI protective layer formed on the Li anode surface.

In conclusion, $LiNO_3$-PAN es can effectively improve the cycle performance of Li metal battery using Cu current collector and Li metal as anode, and shows good practical value as a $LiNO_3$ slow-release interlayer in high-voltage full cell using carbonates electrolyte.

In summary, we have reported a $LiNO_3$-PAN nanowire cloth ($LiNO_3$-PAN es), which can be used as $LiNO_3$ slow-release interlayer in Li metal battery to overcome the disadvantage of low solubility of $LiNO_3$ in carbonate and improve the cycle performance of Li anode. $LiNO_3$-PAN es is fabricated by electrospinning technique, which is a membrane composed of nanowires of $LiNO_3$ dissolved in PAN polymer with a mass ratio of 1:1. By introducing $LiNO_3$-PAN es on Li metal anode's surface, the cycle performance of Li symmetric cell is significantly improved, even when operated at a high current density of 4 mA/cm^2, which contributes to the formation of a single nitrogenous component $Li_2N_2O_2$ SEI layer on Li anode's surface. Such a homogeneous SEI layer can facilitate the uniform deposition of Li^+ and improve the cycle performance of Li anode. In the full cell test, whether Li metal or Cu foil is used as the anode of the battery, $LiNO_3$-PAN es can also effectively enhance the cycle performance of the full cell operated in carbonate electrolyte by enhancing the cycle performance of the anode. This work presents a facile and effective method to introduce abundant $LiNO_3$ into carbonate electrolyte to improve the cycle performance of Li anode.

Declaration of competing interest

The authors declare that they have no known competing financial interests or personal relationships that could have appeared to influence the work reported in this paper.

Acknowledgments

This work was financially supported by the National Key R&D Program of China (No. 2022YFB2402600), National Natural Science Foundation of China (No. 22279166), Basic and Applied Basic Research Foundation of Guangdong Province-Regional joint fund project (No. 2022B1515120019) and the Fundamental Research Funds for the Central Universities, Sun Yat-Sen University (Nos. 22qntd0101 and 22dfx01).

Supplementary materials

Supplementary material associated with this article can be found, in the online version, at doi:10.1016/j.cclet.2023.109274.

References

[1] X.B. Cheng, R. Zhang, C.Z. Zhao, et al., Adv. Sci. 3 (2016) 1500213.
[2] A. Manthiram, X. Yu, S. Wang, Nat. Rev. Mater. 2 (2017) 16103.
[3] H. Wang, X. Cao, H. Gu, et al., ACS Nano 14 (2020) 4601–4608.
[4] T.T. Zuo, X.W. Wu, C.P. Yang, et al., Adv. Mater. 29 (2017) 1700389.
[5] P. Shi, T. Li, R. Zhang, et al., Adv. Mater. 31 (2019) 1807131.
[6] Z. Zeng, V. Murugesan, K.S. Han, et al., Nat. Energy 3 (2018) 674–681.
[7] C.V. Amanchukwu, Z. Yu, X. Kong, et al., J. Am. Chem. Soc. 142 (2020) 7393–7403.
[8] S. Ko, T. Obukata, T. Shimada, et al., Nat. Energy 7 (2022) 1217–1224.
[9] X.Q. Zhang, X. Chen, R. Xu, et al., Angew. Chem. Int. Ed. 56 (2017) 14207–14211.
[10] Y. Jiang, B. Wang, P. Liu, et al., Nano Energy 77 (2020) 105308.
[11] S. Li, J. Huang, Y. Cui, et al., Nat. Nanotechnol. 17 (2022) 613–621.
[12] M. Srout, M. Carboni, J.A. Gonzalez, S. Trabesinger, Small 19 (2023) e2206252.
[13] C. Yan, X.B. Cheng, Y.X. Yao, et al., Adv. Mater. 30 (2018) e1804461.
[14] N.W. Li, Y. Shi, Y.X. Yin, et al., Angew. Chem. Int. Ed. 57 (2018) 1505–1509.
[15] Y. Liu, D. Lin, P.Y. Yuen, et al., Adv. Mater. 29 (2017) 1605531.
[16] Y. Wang, Z. Wang, L. Zhao, et al., Adv. Mater. 33 (2021) e2008133.
[17] X.Q. Zhang, X. Chen, X.B. Cheng, et al., Angew. Chem. Int. Ed. 57 (2018) 5301–5305.
[18] H. Kuwata, H. Sonoki, M. Matsui, Y. Matsuda, N. Imanishi, Electrochemistry 84 (2016) 854–860.
[19] Y. Qian, S. Hu, X. Zou, et al., Energy Storage Mater. 20 (2019) 208–215.
[20] R. May, K.J. Fritzsching, D. Livitz, S.R. Denny, L.E. Marbella, ACS Energy Lett. 6 (2021) 1162–1169.
[21] S. Xiong, K. Xie, Y. Diao, X. Hong, Electrochim. Acta 83 (2012) 78–86.
[22] J. Zhang, H. Zhang, L. Deng, et al., Energy Storage Mater. 54 (2023) 450–460.
[23] Z. Li, H. Rao, R. Atwi, et al., Nat. Commun. 14 (2023) 868.
[24] Z.L. Brown, S. Heiskanen, B.L. Lucht, J. Electrochem. Soc. 166 (2019) A2523–A2527.
[25] C. Yan, Y.X. Yao, X. Chen, et al., Angew. Chem. Int. Ed. 57 (2018) 14055–14059.
[26] Y. Ein-Eli, Electrochem. Solid. St. 2 (1999) 212–214.
[27] E. Peled, D. Golodnitsky, G. Ardel, J. Electrochem. Soc. 144 (1997) L208–L210.
[28] V.R. Rikka, S.R. Sahu, A. Chatterjee, et al., J. Phys. Chem. C 122 (2018) 28717–28726.
[29] Y. Li, Y. Li, A. Pei, et al., Science 358 (2017) 506–510.
[30] X. Shen, R. Zhang, X. Chen, et al., Adv. Energy Mater. 10 (2020) 1903645.
[31] Q. Shi, Y. Zhong, M. Wu, H. Wang, H. Wang, Proc. Natl. Acad. Sci. U. S. A. 115 (2018) 5676–5680.
[32] Y. Liu, X. Qin, D. Zhou, et al., Energy Storage Mater. 24 (2020) 229–236.
[33] Q. Liu, Y. Xu, J. Wang, et al., Nano-Micro Lett. 12 (2020) 176.
[34] S.P. Rwei, T.F. Way, W.Y. Chiang, S.Y. Pan, Colloid Polym, Sci. 295 (2017) 803–815.
[35] N. Chatterjee, S. Basu, S.K. Palit, M.M. Maiti, J. Polym. Sci. Part B: Polym. Phys. 33 (1995) 1705–1712.
[36] S. Gu, S.W. Zhang, J. Han, et al., Adv. Funct. Mater. 31 (2021) 2102128.